Unveiling the Enhancement of Spontaneous Emission at Exceptional Points

L. Ferrier,[1,*] P. Bouteyre,[1,†] A. Pick,[2] S. Cueff,[1] N. H. M Dang,[1] C. Diederichs,[3] A. Belarouci,[1] T. Benyattou,[1] J. X. Zhao,[4] R. Su,[4] J. Xing,[5] Qihua Xiong,[6,7,8] and H. S. Nguyen[1,8,‡]

[1]*Université Lyon, Ecole Centrale de Lyon, CNRS, INSA Lyon, Université Claude Bernard Lyon 1, CPE Lyon, CNRS, INL, UMR5270, 69130 Ecully, France*

[2]*Applied Physics Department, Hebrew University of Jerusalem, Israel*

[3]*Laboratoire de Physique de l'École normale supérieure, ENS, Université PSL, CNRS, Sorbonne Université, Université de Paris, F-75005 Paris, France*

[4]*Division of Physics and Applied Physics, School of Physical and Mathematical Sciences, Nanyang Technological University, Singapore 637371, Singapore*

[5]*College of Chemistry and Molecular Engineering, Qingdao University of Science and Technology, Qingdao 266042, China*

[6]*State Key Laboratory of Low-Dimensional Quantum Physics and Department of Physics, Tsinghua University, Beijing 100084, People's Republic of China*

[7]*Beijing Academy of Quantum Information Sciences, Beijing 100193, People's Republic of China*

[8]*Institut Universitaire de France (IUF), F-75231 Paris, France*

(Received 20 May 2022; accepted 26 July 2022; published 17 August 2022)

Exceptional points (EPs), singularities of non-Hermitian physics where complex spectral resonances degenerate, are one of the most exotic features of nonequilibrium open systems with unique properties. For instance, the emission rate of quantum emitters placed near resonators with EPs is enhanced (compared to the free-space emission rate) by a factor that scales quadratically with the resonance quality factor. Here, we verify the theory of spontaneous emission at EPs by measuring photoluminescence from photonic-crystal slabs that are embedded with a high-quantum-yield active material. While our experimental results verify the theoretically predicted enhancement, they also highlight the practical limitations on the enhancement due to material loss. Our designed structures can be used in applications that require enhanced and controlled emission, such as quantum sensing and imaging.

DOI: 10.1103/PhysRevLett.129.083602

Exploring and taming open, nonconservative systems has always been a major challenge in physics. This relates to a plethora of problems from classical to quantum phenomena: the damping of a pendulum's swing by sliding friction, coherent light escaped from the cavity of a diode laser, harnessing thermal radiation for radiative cooling, and decoherence mechanisms in quantum systems. The past few years have witnessed the triumph of non-Hermtiticy as the modern approach to describing nonconservative mechanisms in a broad range of open systems [1–3]. These systems, theoretically described by non-Hermitian Hamiltonians, would exhibit peculiar features with no Hermitian counterparts. One may cite the non-Hermitian extension of topological matter [4] and the formation of bound states in the continuum resulted from destructive interference of losses [5]. Exceptional points (EPs) are prototypical examples of a unique degeneracy that can occur in non-Hermitian systems [6–9] in which at least two eigenvectors and associate complex eigenvalues simultaneously coalesce. Fundamentally, EPs represent singularities of non-Hermitian topology [10–12]. For instance, in the case of isolated EPs, two eigenstates can be swapped when adiabatically encircling an EP in the parameter space [13–16], a direct consequence of the isolated EPs' half topological charges. Because of their topological nature, many other intriguing phenomena were discovered in systems with EPs such as unidirectional transmission or reflection [8,17,18], loss-induced transparency [19], topological chirality [15,20], and chirality-reversal radiation [21]. For device applications, novel concepts for making sensors with higher sensibility [22–27] and lasers with intriguing properties [28–36] using EP properties have been suggested and implemented.

Recent theoretical work unraveled the mystery regarding the apparent divergence of the emission enhancement at EPs (i.e., the so-called Peterman factor) and predicted unique spectral features with substantial but finite enhancement at EPs [37,38]. However, experimental verification of these results was missing until very recently [39]. In Ref. [39], the authors show that, for the application of sensing, the enhancement of the Petermann factor near the EP is accompanied by a commensurate increase in the noise signal. Therefore, the signal-to-noise ratio is not dramatically improved near the EP, and that limits the applicability of the EP effect in gyro-based sensing applications. While LDOS enhancement near EPs offers limited improvement

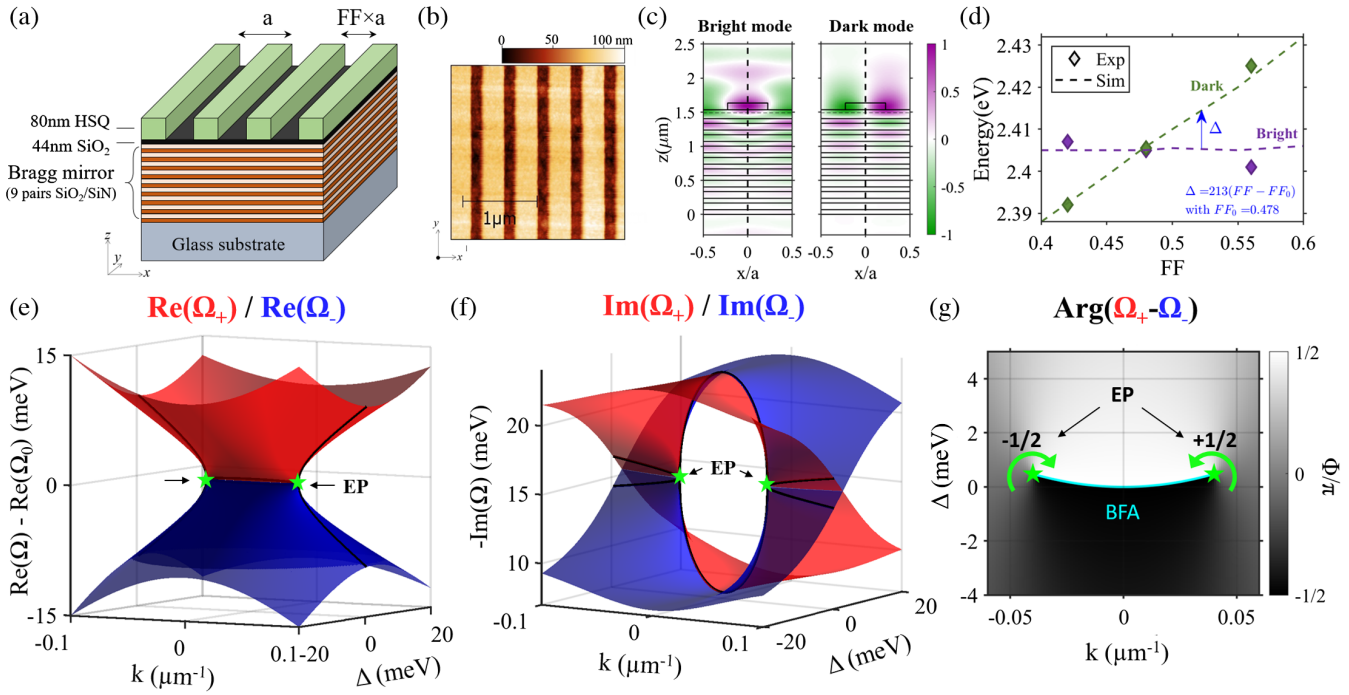

FIG. 1. Sample and analytical model. (a) Sketch of the passive sample composed of a hydrogen silsesquioxane (HSQ) grating on top of a Bragg mirror (nine SiO_2-SiN pairs) with a 44 nm spacing layer of SiO2. The grating period a is 500 nm, with a spacing of $a \times \mathrm{FF}$, with $0 < \mathrm{FF} < 1$ the filling factor. (b) Atomic Force Microscopy (AFM) image of the passive sample. (c) Electric field distribution simulation of the bright and dark modes at wave vector $k = 0$. (d) Energy of the dark and bright modes as a function of the filling factor (FF). The star symbols are experimental data and the lines are results obtained from rigorous-coupled wave analysis simulations [47–49]. (e) and (f) Real and imaginary parts of the system eigenvalues as a function of the wave vector k_x in the direction of the grating, and the energy gap Δ between the two modes. The two EPs, i.e., simultaneous degeneration of the eigenvalues' real and imaginary parts, are indicated with green stars. (g) Argument of the complex gap, $\Phi = \mathrm{Arg}(\Omega_+ - \Omega_-)$, revealing the half-topological charges of EPs. The two yellow points indicate the two isolated EPs and the blue line the bulk Fermi arc (BFA).

in sensing capabilities [39], the implication of EPs for enhanced emission is much more promising since the enhancement of spontaneous emission near EPs in actively pumped structures is theoretically unbounded [38]. Here, we report on the first experimental demonstration of spontaneous emission enhancement at EPs. In particular, we design an experimental platform to demonstrate and analyze the enhancement at EPs taking full account of realistic constraints. The EPs are directly observed from angle-resolved reflectivity measurements, and their LDOS enhancement is revealed via photoluminescence signal when a high-quantum-yield active material is implemented into the system. A finite LDOS enhancement factor was measured and is in perfect agreement with the analytical value predicted by recently proposed theory on LDOS at EPs [38] in the framework of an analytical non-Hermitian model. This result is an essential step toward using EPs in applications as engineering LDOS is at the heart of most of light-matter interaction mechanisms such as accelerating and directing spontaneous emission, tailoring light-harvesting efficiency, enhancing photonic nonlinearity and molding photonic transport.

To engineer isolated EPs, we employ subwavelength unidimensional (1D) photonic lattices exhibiting lateral mirror symmetry $-x \to x$ [see Figs. 1(a) and 1(b)] and study the band structures in the vicinity of the first band gap at Γ point. The two eigenmodes of this gap are transverse electric modes of opposite parities, and are accordingly denoted in the following as dark (antisymmetric) and bright (symmetric) modes [see Fig. 1(c)]. The dark mode cannot couple to the radiative continuum and corresponds to a symmetry protected bound state in the continuum with zero radiative losses [40,41]. Consequently, by playing with a set of two or more uncorrelated parameters, it is possible to make the dark and bright modes coalesce into EPs [40–42]. Using the dark and bright states as a basis, the eigenmodes in the vicinity of Γ can be described by a non-Hermitian kp Hamiltonian (more information in the Supplemental Material [43])

$$H(k,\Delta) = E_0 + \begin{pmatrix} \frac{\Delta+\delta.k^2}{2} & v.k \\ v.k & -\frac{\Delta+\delta.k^2}{2} \end{pmatrix} + i\begin{pmatrix} \gamma_{nr}+\gamma_b & 0 \\ 0 & \gamma_{nr} \end{pmatrix}, \tag{1}$$

In the Hermitian term of (1), Δ is the energy gap between the dark and bright modes, E_0 the midgap energy, δ and v the two coefficients of kp perturbation theory when second

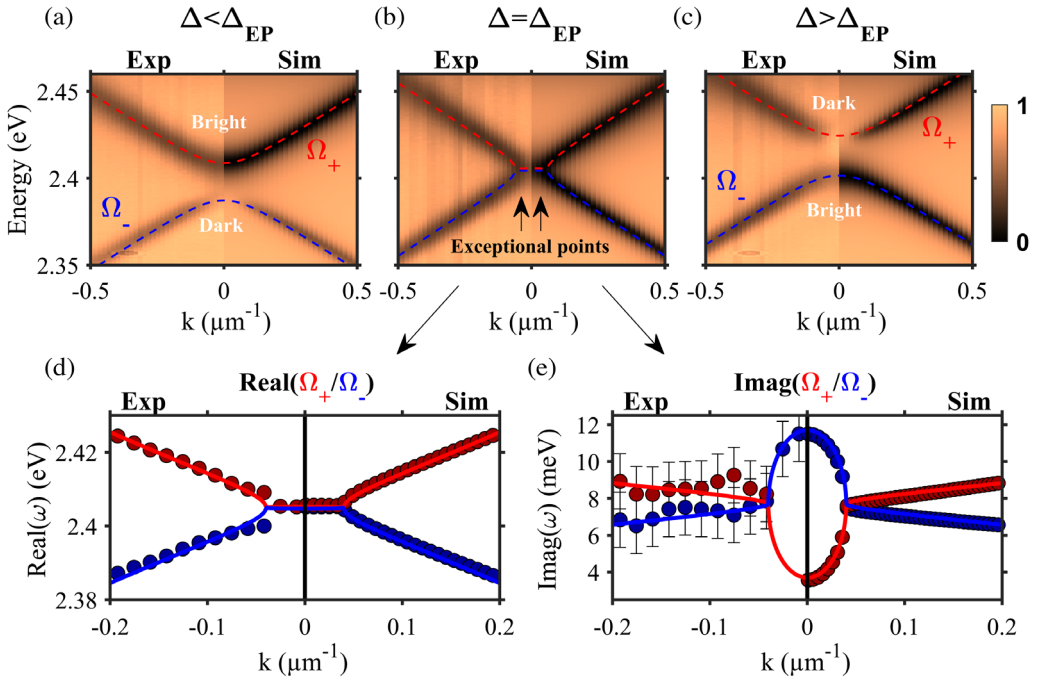

FIG. 2. Experimental investigation on two isolated EPs. (a) to (c), Angle-resolved reflectivity measurements (left panels) and corresponding numerical simulations (right panels) of the sample for $\Delta = -21$ meV (a), $\Delta = 0.48$ meV (b), and $\Delta = 24$ meV (c). (d) and (e) Real and imaginary parts of the experimental (left, dots) and simulated (right, dots) eigenvalues of the structure with EPs in (b) compared with the analytical model (lines) given by (1). At $\Delta = \Delta_{EP}$ and for $k < |k_{EP}|$, the real part of the eigenvalues is almost degenerated, and it is only possible to extract the bright branch from the experimental data. The parameters used for the analytical models are $\Delta = 0.48$ meV, $E_0 = 2.405$ eV, $v = 100$ meV μm^{-1}, $\delta = -300$ meV μm^{-2}, $\gamma_b = 7.5$ meV, and $\gamma_{nr} = 3.8$ meV. The exceptional points are located at ± 0.04 μm^{-1}.

order is included. In the non-Hermitian term of (1), γ_b is the radiative loss of the bright mode and γ_{nr} the nonradiative loss of both modes. Interestingly, together with the wave vector k, the energy gap Δ can be implemented as a synthetic dimension, to form a two-dimensional parameter space $\boldsymbol{q} = (k, \Delta)$. These two parameters are effectively independent of each other as the wave vector k is related to the angle of far-field radiation, whereas the energy gap Δ is dictated by the grating filling factor (FF) [see Fig. 1(d)].

The mapping of the real and imaginary parts of the eigenvalues of (1) are plotted in Figs. 1(e) and 1(f), respectively. One can observe that they are simultaneously degenerated at two EPs of coordinates: $k_{EP} = \pm(\gamma_b/2v_g)$, and $\Delta_{EP} = -\delta.|k_{EP}|$. The isolation and topological nature of these EPs are revealed from the texture of the phase $\Phi(k, \Delta)$ which is defined by the argument of the two eigenvalues complex difference, $\Phi = \arg(\Omega_+ - \Omega_-)$ [10,11]. As shown in Fig. 1(g), one can observe two isolated EPs, both possessing half-topological charges, in the 2D synthetic space. Indeed, encircling each EP accumulates a vortex phase that is equal to $\pm\pi$ [see Fig. 1(g)], with corresponding winding numbers $(1/2\pi)\oint_C d\boldsymbol{q}\nabla_{\boldsymbol{q}}\Phi = \pm\frac{1}{2}$ [10,11]. Finally, these two EPs are connected by a bulk Fermi arc, given by $\Delta = -\delta k^2$, along which the real part of eigenvalues are degenerated [13].

Reflectivity experiments are performed to evidence the two isolated EPs predicted by the analytical model. Figures 2(a)–2(c) present the experimental angle-resolved reflectivity maps (left panels) and the numerically simulated ones (right panels), for three different values of Δ: (a) $\Delta < \Delta_{EP}$, (b) $\Delta = \Delta_{EP}$, and (c) $\Delta > \Delta_{EP}$. In Figs. 2(a) and 2(c), one can easily identify the dark mode for which the radiative resonance vanishes at $k = 0$ due to its antisymmetric parity. These figures also evidence the inversion of the two bands when the difference $\Delta - \Delta_{EP}$ switches sign. Importantly, for $\Delta = \Delta_{EP}$ in Fig. 2(b), the two bands coalesce at two EPs located at $k_{EP} = \pm 0.04$ μm^{-1}. To further confirm the EPs formation, the real and imaginary parts of the eigenvalues are, respectively, retrieved from the spectral position of the resonance dips and their linewidths. These experimental values are depicted in Figs. 2(d) and 2(e), which exhibit a very good agreement with the numerical simulation results and are nicely reproduced by the analytical model.

To probe the LDOS at the isolated EPs, a 15 nm-thick layer of $CsPbBr_3$ perovskite colloidal nanocrystals is deposited on the sample [50]. The choice of this active material is based on two advantages: first, they can sustain near-unity photoluminescence quantum efficiency at the EPs wavelength [51,52], thus, the LDOS is directly

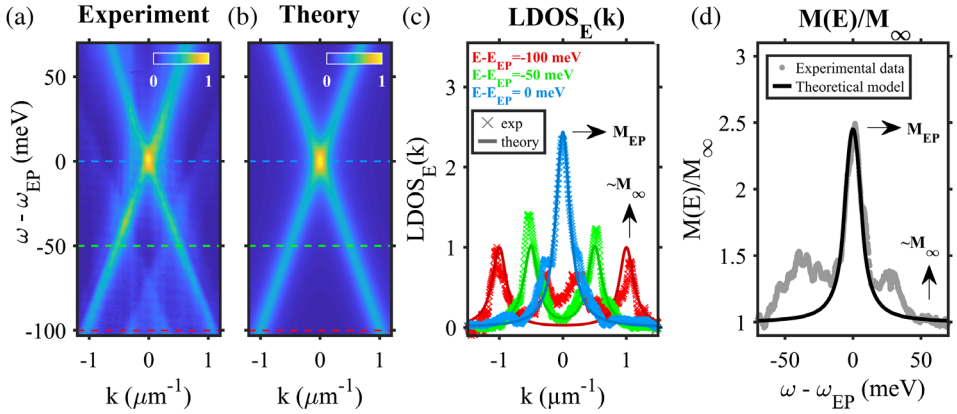

FIG. 3. LDOS enhancement at the EPs. (a) Experimental LDOS map extracted from the photoluminescence measurements of the active sample (sample in Fig. 1(a) with an extra 15 nm-thick $CsPbBr_3$ layer.). (b) Theoretical LDOS map obtained by using the model on the LDOS at EPs in [38] and our analytical model. The parameters used for the theoretical LDOS are $\Delta = 0$ meV, $E_0 = 2.3878$ eV, $v = 100$ meV μm^{-1}, $\delta = 0$ meV μm^{-2}, $\gamma_b = 5$ meV, and $\gamma_{nr} = 11$ meV. (c) Three horizontal isofrequency cross sections, at $\omega - \omega_{EP} = -100$, -50, and 0 meV, of the experimental (crosses) and theoretical (lines) LDOS of (a) and (b). M_{EP} and M_∞, peak values at the energy of the EPs and the nondegenerate resonances, respectively, (i.e., away from the EPs energy) are indicated. (d) Experimental (gray dots) and theoretical (black line) LDOS peak values at given energies, $M(E) = \max_k[\mathrm{LDOS}_E(k)]$, normalized by the LDOS peak value at the nondegenerate resonances away from the exceptional points, M_∞.

proportional to the emission intensity; and second, they can be easily implemented into the passive structure by spin coating with good uniformity.

Figure 3(a) presents the experimental mapping of the LDOS in the vicinity of the EPs, extracted from the angle-resolved photoluminescence measurements. Theoretical predictions, obtained by implementing the Hamiltonian (1) to the LDOS model from Ref. [38], are depicted in Fig. 3(b) and reproduce, remarkably well, the experimental measurements. One can observe from both the experimental and theoretical maps that the LDOS resonate with the photonic modes. Most importantly, the LDOS signal is maximized around the EPs (i.e., at $E = E_{EP}$ and $k = 0$), revealing an enhancement of the LDOS at EPs. Note that the two EPs can no longer be distinguished from one another as the nonradiative losses, γ_{nr}, broaden the two EPs LDOS peaks.

Further insights of the LDOS enhancement are gained by examining its distribution in momentum space at a given energy $\mathrm{LDOS}_E(k)$. Such distribution is simply obtained from an isofrequency cross section of the LDOS map. As an illustration, Fig. 3(c) shows three cross sections of the experimental and theoretical LDOS of Figs. 3(a) and 3(b), corresponding to $E - E_{EP} = -100$, -50, and 0 meV. As for the LDOS maps, again, we have a very good agreement between experiment and theory. From these momentum-resolved distributions, the LDOS peak $M(E) = \max_k[\mathrm{LDOS}_E(k)]$ is retrieved. Figure 3(d) compares the experimental (gray dots) and theoretical (black line) spectrally resolved LDOS peaks. The profile of the experimental $M(E)$ in the vicinity of the EPs' energy is nicely matched to the theoretical $M(E)$ in terms of linewidth and amplitude. For energies away from the EPs' energy, a deviation occurs between experiment and theory. This is explained by the coupling of the nanocrystals emission to additional band-folded Bragg modes [43], which are not considered in our effective theory. Finally, particular attention is paid to the LDOS peaks at the EPs, M_{EP}, and away from the EPs, M_∞, both indicated in Figs. 3(c) and 3(d). The experimental LDOS enhancement corresponds, then, to the ratio between M_{EP} and M_∞ giving a value of 2.56. This experimental finding answers to the fundamental question of the LDOS enhancement at EPs as the enhancement remains finite despite the nonorthogonality of the eigenvectors as predicted in recent theories [38]. Furthermore, the experimental results shown in Fig. 3 are well explained by the theory on LDOS at EPs [38].

In our system, the modal degeneracy at the EP produces an enhancement factor of 2.56. This implies that the intensity at the EP is 2.56 times stronger than that of a single nondegenerate resonance (which is enhanced by the traditional Purcell factor). The excess emission comes from the degeneracy and the nonorthogonality of the modes. Since the enhancement at an ordinary degeneracy is bounded by two, the fact that our enhancement factor exceeding two proves the presence of an EP [53]. This factor of 2.56 can be improved by using high-order passive EPs [37]. Alternatively, by adding gain, this value can also increase at second-order EPs [38]. Although increasing the gain would inevitably increase γ_{nr}, recent work shows that it is possible to achieve high gain with low loss by utilizing hybrid light-matter polaritonic modes that arise from the strong-coupling regime between excitons of quantum wells and photons in photonic crystal [54].

In conclusion, the recent theoretical predictions on the LDOS enhancement at EPs [38] have been confirmed

experimentally while taking full account of realistic constraints from a photonic-crystal slab platform. In our experiment, a finite enhancement factor of 2.56 has been measured and is in good agreement with the one given by our analytical theory. Our results open the way to LDOS engineering in non-Hermitian photonics for novel optoelectronics devices such as lasing operating at EPs when important gain medium is introduced, or nonlinear optics harnessing LDOS enhancement [55]. Finally, while this Letter only studies the radiation of an ensemble of quantum dots at EPs, the effect of EPs on spontaneous emission of single quantum emitters [21] is a salient perspective to explore the new regime of cavity-quantum electrodynamics for novel single photon sources. For example, by performing temporal dynamic experiments on single emitters, our platform could be used to demonstrate the recent prediction from Ref. [56] of the increased lifetime of quantum excitations near EPs.

This work was partly funded by the French National Research Agency (ANR) under the Project POPEYE (Project No. ANR-17-CE24-0020) and the IDEXLYON from Université de Lyon, Scientific Breakthrough project TORE within the Programme Investissements d'Avenir (Project No. ANR-19-IDEX-0005). It is also supported by the Auvergne-Rhône-Alpes region in the framework of PAI2020 and the Vingroup Innovation Foundation (VINIF) annual research grant program under Project No. VINIF.2021.DA00169. Q. X. gratefully acknowledges the funding support from National Natural Science Foundation of China (Grant No. 12020101003) and a Tsinghua University start-up grant. The authors thank Xavier Letartre, Pierre Viktorovitch and Xuan Dung Nguyen for fruitful discussions.

L. Ferrier and P. Bouteyre contributed equally to this Letter as first authors.

*lydie.ferrier@insa-lyon.fr
†paul.bouteyre@ec-lyon.fr
‡hai-son.nguyen@ec-lyon.fr

[1] I. Rotter and J. P. Bird, A review of progress in the physics of open quantum systems: Theory and experiment, Rep. Prog. Phys. **78**, 114001 (2015).
[2] R. El-Ganainy, K. G. Makris, M. Khajavikhan, Z. H. Musslimani, S. Rotter, and D. N. Christodoulides, Non-Hermitian physics and PT symmetry, Nat. Phys. **14**, 11 (2018).
[3] R. El-Ganainy, M. Khajavikhan, D. N. Christodoulides, and S. K. Ozdemir, The dawn of non-Hermitian optics, Commun. Phys. **2**, 37 (2019).
[4] E. J. Bergholtz, J. C. Budich, and F. K. Kunst, Exceptional topology of non-hermitian systems, Rev. Mod. Phys. **93**, 015005 (2021).
[5] C. W. Hsu, B. Zhen, A. D. Stone, J. D. Joannopoulos, and M. Soljačić, Bound states in the continuum, Nat. Rev. Mater. **1**, 16048 (2016).
[6] M. V. Berry and D. H. J. O'Dell, Diffraction by volume gratings with imaginary potentials, J. Phys. A **31**, 2093 (1998).
[7] W. D. Heiss, Phases of wave functions and level repulsion, Eur. Phys. J. D **7**, 1 (1999).
[8] A. Regensburger, C. Bersch, M.-A. Miri, G. Onishchukov, D. N. Christodoulides, and U. Peschel, Parity-time synthetic photonic lattices, Nature (London) **488**, 167 (2012).
[9] L. Ge, Y. D. Chong, and A. D. Stone, Conservation relations and anisotropic transmission resonances in one-dimensional $\mathcal{PT}$-symmetric photonic heterostructures, Phys. Rev. A **85**, 023802 (2012).
[10] H. Shen, B. Zhen, and L. Fu, Topological Band Theory for Non-Hermitian Hamiltonians, Phys. Rev. Lett. **120**, 146402 (2018).
[11] K. Kawabata, T. Bessho, and M. Sato, Classification of Exceptional Points and Non-Hermitian Topological Semimetals, Phys. Rev. Lett. **123**, 066405 (2019).
[12] K. Sone, Y. Ashida, and T. Sagawa, Exceptional non-Hermitian topological edge mode and its application to active matter, Nat. Commun. **11**, 5745 (2020).
[13] H. Zhou, C. Peng, Y. Yoon, C. W. Hsu, K. A. Nelson, L. Fu, J. D. Joannopoulos, M. Soljačić, and B. Zhen, Observation of bulk Fermi arc and polarization half charge from paired exceptional points, Science **359**, 1009 (2018).
[14] T. Gao, E. Estrecho, K. Y. Bliokh, T. C. H. Liew, M. D. Fraser, S. Brodbeck, M. Kamp, C. Schneider, S. Höfling, Y. Yamamoto, F. Nori, Y. S. Kivshar, A. G. Truscott, R. G. Dall, and E. A. Ostrovskaya, Observation of non-Hermitian degeneracies in a chaotic exciton-polariton billiard, Nature (London) **526**, 554 (2015).
[15] J. Doppler, A. A. Mailybaev, J. Böhm, U. Kuhl, A. Girschik, F. Libisch, T. J. Milburn, P. Rabl, N. Moiseyev, and S. Rotter, Dynamically encircling an exceptional point for asymmetric mode switching, Nature (London) **537**, 76 (2016).
[16] Q. Liu, S. Li, B. Wang, S. Ke, C. Qin, K. Wang, W. Liu, D. Gao, P. Berini, and P. Lu, Efficient Mode Transfer on a Compact Silicon Chip by Encircling Moving Exceptional Points, Phys. Rev. Lett. **124**, 153903 (2020).
[17] Z. Lin, H. Ramezani, T. Eichelkraut, T. Kottos, H. Cao, and D. N. Christodoulides, Unidirectional Invisibility Induced by $\mathcal{PT}$-Symmetric Periodic Structures, Phys. Rev. Lett. **106**, 213901 (2011).
[18] B. Peng, Ş.K. Özdemir, F. Lei, F. Monifi, M. Gianfreda, G. L. Long, S. Fan, F. Nori, C. M. Bender, and L. Yang, Parity-time-symmetric whispering-gallery microcavities, Nat. Phys. **10**, 394 (2014).
[19] A. Guo, G. J. Salamo, D. Duchesne, R. Morandotti, M. Volatier-Ravat, V. Aimez, G. A. Siviloglou, and D. N. Christodoulides, Observation of $\mathcal{PT}$-Symmetry Breaking in Complex Optical Potentials, Phys. Rev. Lett. **103**, 093902 (2009).
[20] H. Xu, D. Mason, L. Jiang, and J. G. E. Harris, Topological energy transfer in an optomechanical system with exceptional points, Nature (London) **537**, 80 (2016).
[21] H.-Z. Chen, T. Liu, H.-Y. Luan, R.-J. Liu, X.-Y. Wang, X.-F. Zhu, Y.-B. Li, Z.-M. Gu, S.-J. Liang, H. Gao, L. Lu, L. Ge, S. Zhang, J. Zhu, and R.-M. Ma, Revealing the missing

dimension at an exceptional point, Nat. Phys. **16**, 571 (2020).
[22] J. Wiersig, Enhancing the Sensitivity of Frequency and Energy Splitting Detection by Using Exceptional Points: Application to Microcavity Sensors for Single-Particle Detection, Phys. Rev. Lett. **112**, 203901 (2014).
[23] H. Hodaei, A. U. Hassan, S. Wittek, H. Garcia-Gracia, R. El-Ganainy, D. N. Christodoulides, and M. Khajavikhan, Enhanced sensitivity at higher-order exceptional points, Nature (London) **548**, 187 (2017).
[24] P.-Y. Chen and J. Jung, $\mathcal{PT}$ Symmetry and Singularity-Enhanced Sensing Based on Photoexcited Graphene Metasurfaces, Phys. Rev. Applied **5**, 064018 (2016).
[25] W. Chen, S. Kaya Ozdemir, G. Zhao, J. Wiersig, and L. Yang, Exceptional points enhance sensing in an optical microcavity, Nature (London) **548**, 192 (2017).
[26] J.-H. Park, A. Ndao, W. Cai, L. Hsu, A. Kodigala, T. Lepetit, Y.-H. Lo, and B. Kanté, Symmetry-breaking-induced plasmonic exceptional points and nanoscale sensing, Nat. Phys. **16**, 462 (2020).
[27] Z. Dong, Z. Li, F. Yang, C.-W. Qiu, and J. S. Ho, Sensitive readout of implantable microsensors using a wireless system locked to an exceptional point, National electronics review **2**, 335 (2019).
[28] P. Miao, Z. Zhang, J. Sun, W. Walasik, S. Longhi, N. M. Litchinitser, and L. Feng, Orbital angular momentum microlaser, Science **353**, 464 (2016).
[29] Z. Gao, S. T. M. Fryslie, B. J. Thompson, P. S. Carney, and K. D. Choquette, Parity-time symmetry in coherently coupled vertical cavity laser arrays, Optica **4**, 323 (2017).
[30] Z. Gu, N. Zhang, Q. Lyu, M. Li, S. Xiao, and Q. Song, Experimental demonstration of PT-symmetric stripe lasers, Laser Photonics Rev. **10**, 588 (2016).
[31] H. Hodaei, M.-A. Miri, M. Heinrich, D. N. Christodoulides, and M. Khajavikhan, Parity-time–symmetric microring lasers, Science **346**, 975 (2014).
[32] L. Feng, Z. J. Wong, R.-M. Ma, Y. Wang, and X. Zhang, Single-mode laser by parity-time symmetry breaking, Science **346**, 972 (2014).
[33] B. Peng, Ş. K. Özdemir, M. Liertzer, W. Chen, J. Kramer, H. Yılmaz, J. Wiersig, S. Rotter, and L. Yang, Chiral modes and directional lasing at exceptional points, Proc. Natl. Acad. Sci. U.S.A. **113**, 6845 (2016).
[34] M. Liertzer, L. Ge, A. Cerjan, A. D. Stone, H. E. Türeci, and S. Rotter, Pump-Induced Exceptional Points in Lasers, Phys. Rev. Lett. **108**, 173901 (2012).
[35] B. Peng, Ş. K. Özdemir, S. Rotter, H. Yilmaz, M. Liertzer, F. Monifi, C. M. Bender, F. Nori, and L. Yang, Loss-induced suppression and revival of lasing, Science **346**, 328 (2014).
[36] M. Brandstetter, M. Liertzer, C. Deutsch, P. Klang, J. Schöberl, H. E. Türeci, G. Strasser, K. Unterrainer, and S. Rotter, Reversing the pump dependence of a laser at an exceptional point, Nat. Commun. **5**, 4034 (2014).
[37] Z. Lin, A. Pick, M. Lončar, and A. W. Rodriguez, Enhanced Spontaneous Emission at Third-Order Dirac Exceptional Points in Inverse-Designed Photonic Crystals, Phys. Rev. Lett. **117**, 107402 (2016).
[38] A. Pick, B. Zhen, O. D. Miller, C. W. Hsu, F. Hernandez, A. W. Rodriguez, M. Soljačić, and S. G. Johnson, General theory of spontaneous emission near exceptional points, Opt. Express **25**, 12325 (2017).
[39] H. Wang, Y.-H. Lai, Z. Yuan, M.-G. Suh, and K. Vahala, Petermann-factor sensitivity limit near an exceptional point in a Brillouin ring laser gyroscope, Nat. Commun. **11**, 1610 (2020).
[40] S.-G. Lee and R. Magnusson, Band flips and bound-state transitions in leaky-mode photonic lattices, Phys. Rev. B **99**, 045304 (2019).
[41] L. Lu, Q. Le-Van, L. Ferrier, E. Drouard, C. Seassal, and H. S. Nguyen, Engineering a light-matter strong coupling regime in perovskite-based plasmonic metasurface: Quasi-bound state in the continuum and exceptional points, Photonics Res. **8**, A91 (2020).
[42] B. Zhen, C. W. Hsu, Y. Igarashi, L. Lu, I. Kaminer, A. Pick, S.-L. Chua, J. D. Joannopoulos, and M. Soljačić, Spawning rings of exceptional points out of dirac cones, Nature (London) **525**, 354 (2015).
[43] See Supplemental Material at http://link.aps.org/supplemental/10.1103/PhysRevLett.129.083602 for details of: (i) the theoretical models (theory of LDOS at EPs, effective theory of non-Hermitian 1D photonic lattice), (ii) sample fabrication, (iii) experimental and numerical methods, (iv) demonstration of encircling the EPs of the passive structure, (v) LDOS extraction from photoluminescence signal, (vi) effect of nonradiative losses on LDOS enhancement at EP, which includes Refs. [44–46].
[44] G. B. Arfken and H. J. Weber, *Mathematical Methods for Physicists* (Elsevier Academic Press, Boston, 2006), pp. 184–185.
[45] E. Hernàndez, A. Jàuregui, and A. Mondragòn, Jordan blocks and Gamow-Jordan eigenfunctions associated with a degeneracy of unbound states, Phys. Rev. A **67**, 022721 (2003).
[46] A. Taflove, A. Oskooi, and S. G. Johnson, *Advances in FDTD Computational Electrodynamics: Photonics and Nanotechnology* (Artech House, Norwood, MA, 2013), p. 76.
[47] V. Liu and S. Fan, S4: A free electromagnetic solver for layered periodic structures, Comput. Phys. Commun. **183**, 2233 (2012).
[48] M. G. Moharam and T. K. Gaylord, Rigorous coupled-wave analysis of metallic surface-relief gratings, J. Opt. Soc. Am. A **3**, 1780 (1986).
[49] D. Alonso-Álvarez, T. Wilson, P. Pearce, M. Führer, D. Farrell, and N. Ekins-DaukesSolcore: A multi-scale, python-based library for modelling solar cells and semiconductor materials, J. Comput. Electron. **17**, 1099 (2018).
[50] L. Protesescu, S. Yakunin, M. I. Bodnarchuk, F. Krieg, R. Caputo, C. H. Hendon, R. X. Yang, A. Walsh, and M. V. Kovalenko, Nanocrystals of cesium lead halide perovskites (CsPbX3, X = Cl, Br, and I): Novel optoelectronic materials showing bright emission with wide color gamut, Nano Lett. **15**, 3692 (2015).
[51] F. Di Stasio, S. Christodoulou, N. Huo, and G. Konstantatos, Near-unity photoluminescence quantum yield in CsPbBr3 nanocrystal solid-state films via postsynthesis treatment with lead bromide, Chem. Mater. **29**, 7663 (2017).
[52] A. F. Gualdrón-Reyes, S. Masi, and I. Mora-Seró, Progress in halide-perovskite nanocrystals with near-unity photoluminescence quantum yield, Trends Chem. **3**, 499 (2021).

[53] The emission lineshape at an EP is a squared Lorentzian while that of an ordinary degeneracy is a Lorentzian multiplied by the degree of degeneracy; in this case, 2.
[54] V. Ardizzone, F. Riminucci, S. Zanotti, A. Gianfrate, M. Efthymiou-Tsironi, D. G. Suàrez-Forero, F. Todisco, M. De Giorgi, D. Trypogeorgos, G. Gigli, K. Baldwin, L. Pfeiffer, D. Ballarini, H. S. Nguyen, D. Gerace, and D. Sanvitto, Polariton Bose–Einstein condensate from a bound state in the continuum, Nature (London) **605**, 447 (2022).
[55] M. Benzaouia, A. D. Stone, and S. G. Johnson, Nonlinear exceptional-point lasing, arXiv:2206.12969.
[56] M. Khanbekyan and J. Wiersig, Decay suppression of spontaneous emission of a single emitter in a high-q cavity at exceptional points, Phys. Rev. Research **2**, 023375 (2020).